COMMUNICATION

Check for updates

IrRu nanoparticles boosted by Ir/Ru–N–C for acidic hydrogen oxidation with high CO tolerance

Mengyu Yang,[a] Rui Gao, (iD) *[a] Shuo Han,[a] Zhongyu Qiu,[a] Chunxiao Chai,[a] Hao Yang,[a] Yang Zhao,[b] Ruijie Song,[a] Xihong Shen,[a] Xingchen Zeng[a] and Yujiang Song (iD) *[a]

IrRu nanoparticles surrounded by Ir/Ru–N–C retain 91.68% of the initial current density at 0.1 V *vs.* RHE toward acidic hydrogen oxidation reaction in the presence of 1000 ppm CO/H_2, closely correlated with the removal of CO *via* the following reaction: CO_{ad}–IrRu nanoparticle + OH_{ad}–Ir/Ru–N–C → $COOH_{ad}$.

Proton exchange membrane fuel cells (PEMFCs) are attractive energy conversion devices owing to low emissions, sustainability, high energy efficiency, environmental adaptability, fast fueling, and high energy density.[1–6] Currently, high-purity hydrogen (≥99.999%) has regularly been employed in PEMFCs. However, it is costly (US$ 6.07–7.23 kg^{-1}) and has largely impeded the widespread application of PEMFCs.[7–11] It is desirable to operate PEMFCs with low-cost crude H_2 (US$ 0.5–1.7 kg^{-1}).[12,13] Unfortunately, crude H_2 frequently comes from reformed fossil fuels and unavoidably contains CO impurities. State-of-the-art Pt/C electrocatalysts for the acidic hydrogen oxidation reaction (HOR) are susceptible to trace amounts of CO (10 ppm) because the binding energy of CO_{ad} is stronger than that of H_{ad}, seriously obstructing the adsorption and oxidation of H_2.[14–17]

Significant efforts have been contributed to improve the CO tolerance. Gautam *et al.* synthesized carbon-supported PtRuAuPd alloy to tune the electronic structure of Pt, thus weakening the CO adsorption energy.[18] Dong *et al.* delicately combined PtNiMo alloy and Fe–N–C substrate to downshift the d-band centre of Pt and weaken CO adsorption.[19] Long *et al.* tactfully constructed Pt clusters with neighbouring Ru single atoms on MoC_x to promote H_2O dissociation into OH_{ad} at Ru and MoC_x sites, thus enabling the CO oxidation reaction (COOR, CO_{ad}–Pt

clusters + OH_{ad}–MoC_x/Ru–N–C → $COOH_{ad}$) at 0.31 V *vs.* RHE.[20] Shen *et al.* skilfully loaded Pt clusters on hollow bowl-like W_3O/WC to allow CO adsorption at Pt and H_2O dissociation into OH_{ad} at W sites for COOR at 0.81 V *vs.* RHE.[21] Regardless of the considerable progress,[22–25] it is imperative to endow electrocatalysts with COOR capability at a low potential.

Herein, we report the synthesis of IrRu nanoparticles (NPs) encompassing by atomically dispersed Ir/Ru (Ir/Ru–N–C) *via* the simple pyrolysis of zeolitic imidazolate framework-8 (ZIF-8) with enclosed iridium acetylacetonate (Ir(acac)$_3$) and ruthenium acetylacetonate (Ru(acac)$_3$). Remarkably, the nanocomposite demonstrates 91.68% retention of the initial current density at 0.1 V *vs.* RHE ($j_{0.1}$) in 1000 ppm CO/H_2-saturated 0.5 M H_2SO_4 aqueous solution (aq.), far surpassing commercial Pt/C (23.12%). The CO resistance originates from the low onset potential of COOR (0.09 V *vs.* RHE), possibly owing to weakened CO_{ad} on IrRu NPs in combination with OH_{ad} at Ir/Ru–N–C sites produced by H_2O dissociation. Furthermore, the nanocomposite and commercial Pt/C fabricated HOR electrode displays a current density of 0.59 A cm^{-2} at 0.6 V in PEMFCs with 50 ppm CO/H_2 as the fuel, which is 2.5 times that of a Pt/C-based HOR electrode. To the best of our knowledge, this is the first study to couple IrRu NPs with Ir/Ru–N–C for weakening CO adsorption and promoting its oxidation during the acidic HOR process.

In a typical synthesis process, Ir(acac)$_3$ and Ru(acac)$_3$ methanolic solution was firstly mixed with 2-methylimidazole aqueous solution. Next, Zn acetate and polyvinylpyrrolidone aqueous solution was added, and the mixture was stirred for 4 h under ambient conditions. Afterwards, the orange-reddish precipitates formed in the reaction mixture were collected by centrifugation and purified with ultrapure water, followed by drying overnight at 75 °C. Eventually, the powder was heat-treated at 900 °C for 2 h under an argon atmosphere (see more details[26] in the SI and Fig. S1). By varying the molar ratio of Ir(acac)$_3$ to Ru(acac)$_3$ and the

[a] State Key Laboratory of Fine Chemicals, School of Chemical Engineering, Dalian University of Technology, 2 Linggong Road, Dalian, Liaoning, 116024, China. E-mail: gaorui16@dlut.edu.cn, yjsong@dlut.edu.cn
[b] Dalian National Laboratory for Clean Energy, Dalian Institute of Chemical Physics, Chinese Academy of Sciences, Dalian, Liaoning, 116023, China

pyrolysis temperature, a series of electrocatalysts was prepared for comparison.

High-resolution scanning transmission electron microscopy (HR-STEM) reveals that ultrafine and uniformly dispersed NPs with an average diameter of 1.9 ± 0.4 nm have been synthesized, as shown in Fig. 1a and S2. Occasionally, a small number of particles with a diameter of 10–20 nm are noticed in the sample (Fig. S3).

Furthermore, high-angle annular dark field-STEM (HAADF-STEM) shows that NPs are encompassed by a large number of isolated bright dots (Fig. 1b, c and S4). Energy dispersive X-ray spectroscopy (EDS) elemental mapping and the linear scanning profile show the homogeneous distribution of Ir and Ru in the NPs and the uniform distribution of Ir, Ru, and N in the C matrix (Fig. 1c–g and S5). This indicates the formation of IrRu alloy NPs and atomically dispersed Ir sites and Ru sites, more than likely as Ir/Ru–N–C.[27,28] In addition, inductively coupled plasma-optical emission spectroscopy (ICP-OES) shows that the Ir and Ru content in the nanocomposite are 8.48 wt% and 3.19 wt%, respectively (Fig. S6). Moreover, HAADF-STEM reveals that the IrRu NPs are face-centred cubic (fcc) nanocrystals

with a typical lattice spacing of 0.22 nm along the (111) plane (Fig. 1h and S7). X-ray diffraction (XRD) again verifies the fcc structure of the IrRu NPs, with characteristic diffraction peaks of (111), (200), (220), and (311) plane locating at 40.7°, 47.3°, 69.4° and 83.8°, respectively (Fig. 1i).

The HOR activity and CO tolerance of the nanocomposite were assessed in 0.5 M H_2SO_4 aq. As shown in Fig. 2a–c and S8, the nanocomposite exhibits a $j_{0.1}$ and Tafel slope values of 3.11 mA cm^{-2} and 20.12 mV dec^{-1} in pure H_2, respectively, which are comparable to those of commercial Pt/C (2.54 mA cm^{-2} and 35.73 mV dec^{-1}) and commercial PtRu/C (2.64 mA cm^{-2} and 35.17 mV dec^{-1}). This indicates that the nanocomposite has reasonably good activity and kinetics toward acidic HOR. More importantly, the CO tolerance was evaluated by holding the working electrode of the nanocomposite at 0.1 V vs. RHE for 600 s in 1000 ppm CO/H_2-saturated 0.5 M H_2SO_4 aq. and then recording the HOR polarization curves. Relative to the sample with no CO poisoning, the nanocomposite retains 99.04% of $j_{0.1}$, surpassing commercial Pt/C (90.16%), commercial PtRu/C (89.77%), and reported electrocatalysts in the literature (Fig. 2d, e
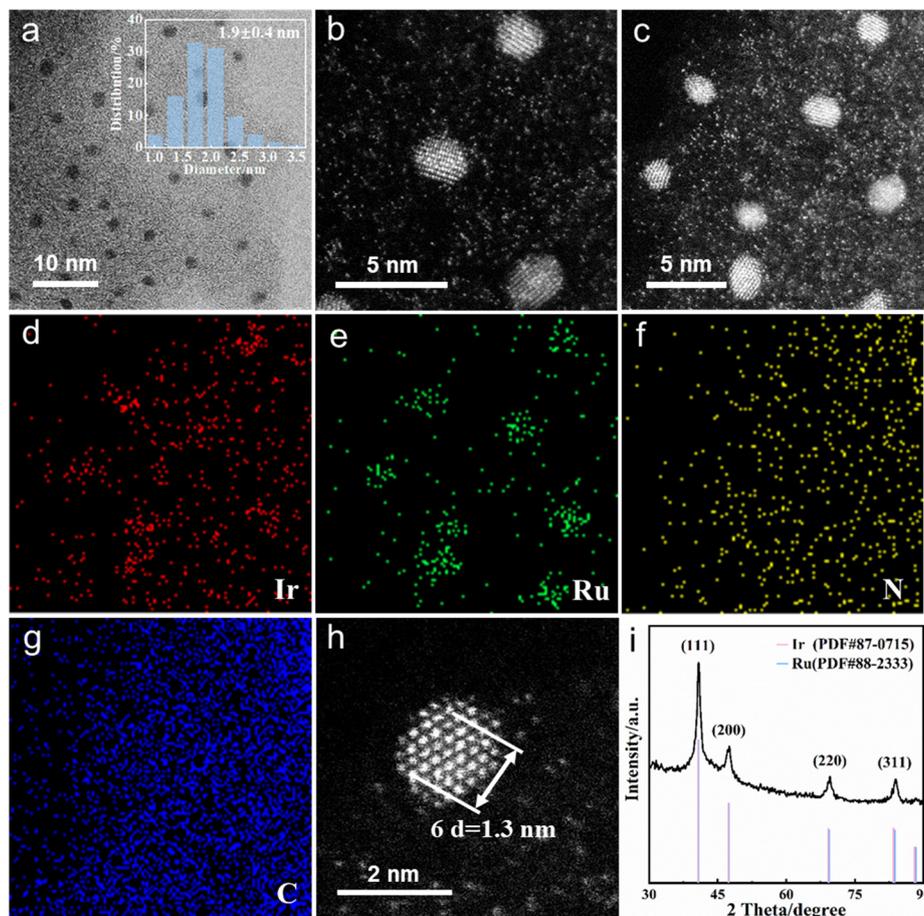

Fig. 1 (a–c) Typical HR-STEM and HAADF–STEM images of the nanocomposite; (d–g) EDS elemental mapping of Ir, Ru, N, and C; (h) HAADF–STEM image of an individual IrRu NP; and (i) the XRD pattern of the nanocomposite; the inset in (a) shows the size distribution of IrRu NPs based on manually measuring 125 individual particles.
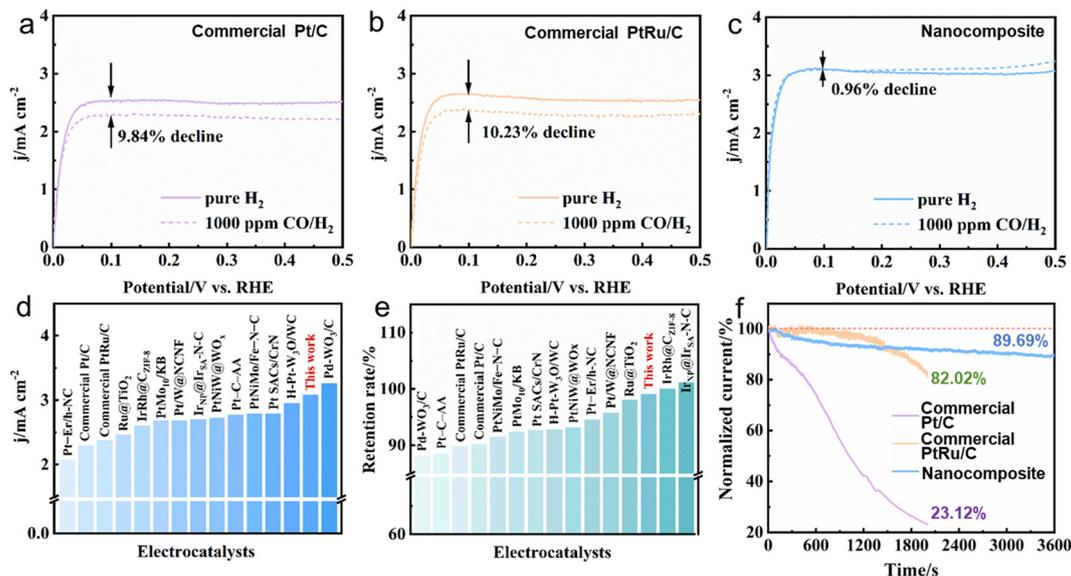
Fig. 2 (a–c) HOR polarization curves of commercial Pt/C, commercial PtRu/C, and the nanocomposite in 0.5 M H_2SO_4 aq. with/without 1000 ppm CO; (d and e) $j_{0.1}$ values in 1000 ppm CO/H_2-saturated electrolytes and corresponding retention rates of the nanocomposite and reported noble-metal-based HOR electrocatalysts; and (f) chronoamperometry curves at 0.1 V *vs.* RHE of commercial Pt/C, commercial PtRu/C, and the nanocomposite in 1000 ppm CO/H_2-saturated 0.5 M H_2SO_4 aq.

and Table S1). Furthermore, the nanocomposite retains 91.68% and 89.69% of $j_{0.1}$ even after holding the potential at 0.1 V *vs.* RHE for 2000 s and 3600 s, respectively, in 1000 ppm CO/H_2-saturated 0.5 M H_2SO_4 aq., demonstrating performance competitive with those reported in the literature (Fig. 2f, and Table S2). In contrast, commercial Pt/C and commercial PtRu/C retain 23.12% and 82.02% of $j_{0.1}$, respectively, after 2000 s of operation. This confirms that the

nanocomposite possesses excellent resistance to CO poisoning. Meanwhile, the molar ratio of Ir/Ru precursors and the pyrolysis temperature are critical in determining the HOR activity and CO tolerance. The molar ratio of Ir(acac)$_3$/Ru(acac)$_3$ of 2 : 1 and pyrolysis temperature of 900 °C are the best parameters by comparing $j_{0.1}$ and the corresponding attenuation values in 0.5 M H_2SO_4 aq. with/without 1000 ppm CO, as shown in Fig. S9–S13.
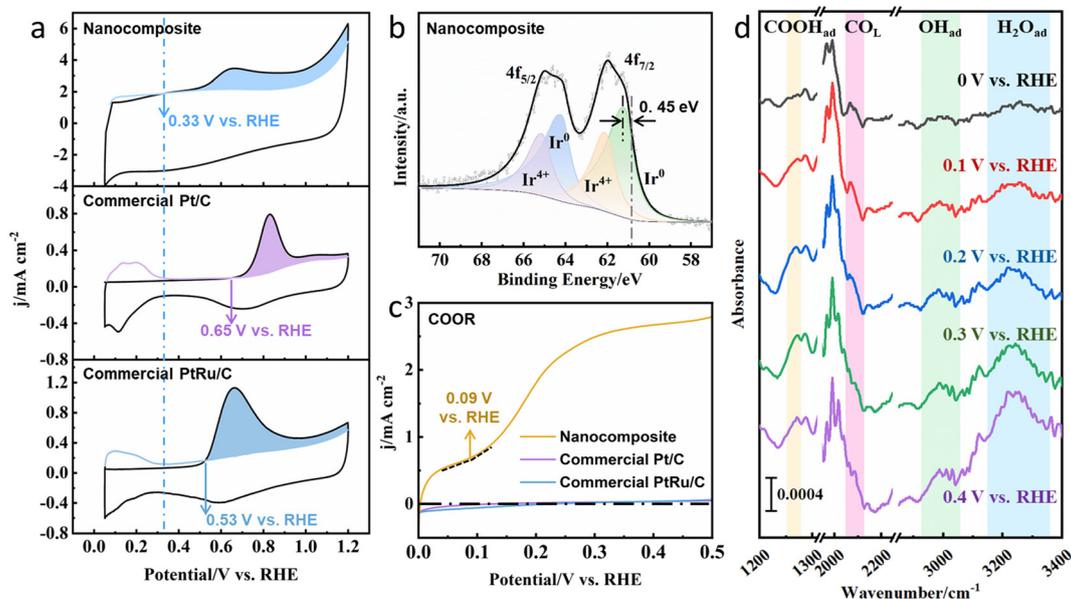

Fig. 3 (a) CO-stripping curves of the nanocomposite, commercial Pt/C, and commercial PtRu/C; (b) Ir 4f XPS of the nanocomposite; (c) COOR polarization curves of the nanocomposite, commercial Pt/C, and commercial PtRu/C in CO-saturated 0.5 M H_2SO_4 aq.; and (d) *in situ* ATR-SEIRAS of the nanocomposite in CO-saturated 0.5 M H_2SO_4 aq.

It is imperative to gain more insights into the origin of the CO resistance. According to CO-stripping measurements in Fig. 3a, the electrochemically active surface area (ECSA) of the nanocomposite was determined to be 141.7 m^2 g$_{IrRu}^{-1}$, larger than that of commercial Pt/C (102.2 m^2 g$_{Pt}^{-1}$) and comparable to that of commercial PtRu/C (168.6 m^2 g$_{PtRu}^{-1}$). The high ECSA should be a contributor to the good electrocatalytic ability of the nanocomposite. We further studied the CO desorption onset potential (E_{CO}) recorded from the CO-stripping curves. Relative to commercial Pt/C (0.65 V vs. RHE) and commercial PtRu/C (0.53 V vs. RHE), the E_{CO} of the nanocomposite negatively shifts to 0.33 V vs. RHE, implying weakened CO adsorption on the active sites. Furthermore, Ir 4f X-ray photoelectron spectroscopy (XPS) of the nanocomposite shows a characteristic doublet of Ir 4f$_{7/2}$ and Ir 4f$_{5/2}$ that can be further deconvoluted into two pairs of doublets (Ir^0 and Ir^{4+}), as shown in Fig. 3b. The Ir^0 4f$_{7/2}$ binding energy of the nanocomposite (61.25 eV) positively shifts by 0.45 eV relative to that of standard metallic Ir (60.8 eV),[29] which is indicative of the electron loss by Ir. This is beneficial for weakening the adsorption of CO on the nanocomposite.
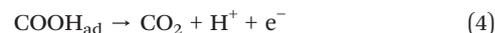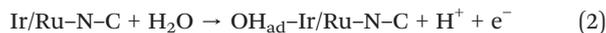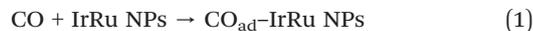
Moreover, electrocatalytic COOR ability of the above electrocatalyst was taken into account (Fig. 3c). It is found that the nanocomposite demonstrates an onset potential of 0.09 V vs. RHE toward COOR in CO-saturated 0.5 M H$_2$SO$_4$ aq. In stark contrast, the electrocatalytic COOR hardly occurs at potential lower than 0.5 V vs. RHE for commercial Pt/C and commercial PtRu/C. We are only aware that IrRh@C$_{ZIF-8}$ and Ir/Ru–N–C also exhibit a low onset potential toward COOR in CO-saturated 0.1 M HClO$_4$ aq.[30,31]

To further investigate the role of IrRu NPs, carbon-supported IrRu NPs (IrRu/C) were synthesized via simple chemical reduction of IrCl$_3$ and RuCl$_3$ in NaBH$_4$ aqueous solution, as shown in Fig. S14a.[32] The strongest X-ray diffraction peak of IrRu/C is located between that of metallic Ir and Ru (Fig. S14b), which suggests the formation of IrRu alloy structure. However, IrRu/C only retains 83.56% of initial $j_{0.1}$ in the presence of 1000 ppm CO, as shown in Fig. S15a, which is much lower than that of IrRu NPs + Ir/Ru–N–C. Moreover, IrRu/C has no activity toward COOR (Fig. S15b). Apparently, Ir/Ru–N–C brings in COOR activity and thus improves the CO resistance.

In addition, in situ attenuated total reflection surface-enhanced infrared absorption spectroscopy (ATR-SEIRAS) was employed to probe the COOR intermediates in CO-saturated 0.5 M H$_2$SO$_4$ aq. At different potentials, the nanocomposite displays the vibration band of linear-adsorbed CO (CO$_L$) at 2070 cm^{-1} (Fig. 3d). Meanwhile, the bands of COOH$_{ad}$, OH$_{ad}$, and H$_2$O$_{ad}$ are observed at 1260–1280 cm^{-1}, 2920–3050 cm^{-1}, and 3150–3340 cm^{-1}, respectively.

Therefore, we propose that IrRu nanoparticles more than likely adsorb CO (step 1). The surrounding Ir/Ru–N–C sites promote H$_2$O dissociation into OH$_{ad}$ (step 2), which combines with CO$_{ad}$ to form COOH$_{ad}$ (step 3) that further

deprotonates to form CO$_2$ (step 4). Such a mechanism is in good agreement with previous studies on improving COOR activity via single-atom electrocatalysts.[16,30,31] In our case, it is possible that the IrRu nanoparticles and Ir/Ru–N–C sites cooperatively remove CO$_{ad}$, thus improving the CO resistance.

$$CO + IrRu\ NPs \rightarrow CO_{ad}\text{–}IrRu\ NPs \quad (1)$$

$$Ir/Ru\text{–}N\text{–}C + H_2O \rightarrow OH_{ad}\text{–}Ir/Ru\text{–}N\text{–}C + H^+ + e^- \quad (2)$$

$$CO_{ad}\text{–}IrRu\ NPs + OH_{ad}\text{–}Ir/Ru\text{–}N\text{–}C \rightarrow COOH_{ad} \quad (3)$$

$$COOH_{ad} \rightarrow CO_2 + H^+ + e^- \quad (4)$$

The excellent CO tolerance of the nanocomposite was verified in PEMFCs. Gas diffusion layer coated with 0.02 mg$_{IrRu}$ cm^{-2} of the nanocomposite and membrane coated with 0.1 mg$_{Pt}$ cm^{-2} of commercial 60 wt% Pt/C were used to construct CO-resistant HOR electrode (Fig. S16). Under conditions of 50 ppm CO/H$_2$–O$_2$, PEMFCs achieves a peak power density of 489 mW cm^{-2} and a current density of 0.59 A cm^{-2} at 0.6 V, which are much superior to a Pt/C-based PEMFCs (300 mW cm^{-2}, 0.24 A cm^{-2}), as shown in Fig. 4a, b and S17. Additionally, by replacing commercial 60 wt% Pt/C with commercial 30 wt% PtRu/C (0.1 mg$_{PtRu}$ cm^{-2}) in the anodic catalyst layer, the PEMFCs demonstrate a current density of 0.67 A cm^{-2} at 0.6 V, which is 5.2 times that of commercial PtRu/C-based PEMFCs (0.13 A cm^{-2}, Fig. 4c and d). The durability of the nanocomposite + PtRu/C-based HOR electrode was tested by holding it at 0.65 V for 5 h under conditions of 50 ppm CO/H$_2$–O$_2$. The PEMFC exhibits a current retention of 36.67% (Fig. S18). In addition, the nanocomposite-based PEMFCs with 0.1 mg$_{IrRu}$ cm^{-2} achieve a current density of 0.34 A cm^{-2} at 0.6 V (Fig. S19),
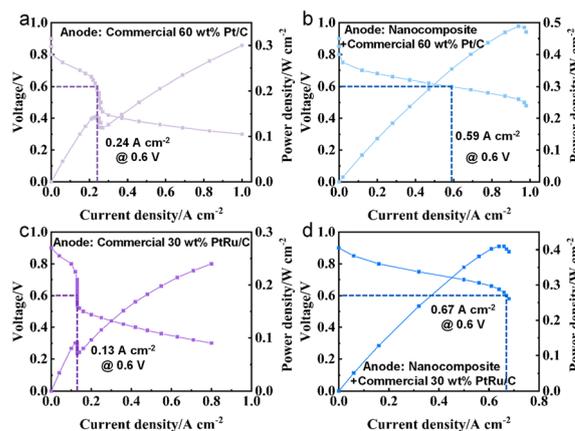

Fig. 4 (a–d) PEMFC single-cell performance with commercial 60 wt% Pt/C, the nanocomposite and commercial 60 wt% Pt/C, commercial 30 wt% PtRu/C, and the nanocomposite and commercial 30 wt% PtRu/C as anodic electrocatalysts, respectively. All PEMFC single cells operated at 80 °C at 150 kPa with 50 ppm CO/H$_2$ and O$_2$.

104 | Catal. Sci. Technol., 2026, 16, 101–106

This journal is © The Royal Society of Chemistry 2026

which is also higher than that of commercial-Pt/C- and PtRu/C-based PEMFCs.

Conclusions

In summary, IrRu NPs surrounded by atomically dispersed Ir/Ru–N–C exhibit excellent CO tolerance toward acidic HOR in terms of maintaining 91.68% of $j_{0.1}$ after holding the potential at 0.1 V $vs.$ RHE for 2000 s in 1000 ppm CO/H$_2$-saturated 0.5 M H$_2$SO$_4$ aq. According to CO-stripping curves and XPS, electron loss of Ir contributes to the weakened adsorption of CO on the nanocomposite. COOR assessments and $in\ situ$ ATR-SEIRAS confirm that H$_2$O dissociation into OH$_{ad}$ at Ir/Ru–N–C sites is beneficial for the oxidation and removal of adsorbed CO on IrRu NPs at 0.09 V $vs.$ RHE. This work provides an effective strategy for improving the CO resistance of HOR electrocatalysts by endowing them with good COOR capabilities.

Author contributions

Mengyu Yang: conceptualization, data curation, investigation, formal analysis, writing – original draft. Rui Gao: resources, conceptualization, writing – original draft, writing – review & editing, project administration. Shuo Han: resources, data curation. Zhongyu Qiu: resources. Chunxiao Chai: resources. Hao Yang: resources. Yang Zhao: resources. Ruijie Song: investigation. Xihong Shen: investigation. Xingchen Zeng: investigation. Yujiang Song: supervision, project administration, writing – review & editing.

Conflicts of interest

There are no conflicts to declare.

Data availability

The data supporting this article have been included as part of the supplementary information (SI). Supplementary information is available. See DOI: https://doi.org/10.1039/d5cy01144b.

Acknowledgements

Notes and references

1 K. Jiao, J. Xuan, Q. Du, Z. Bao, B. Xie, B. Wang, Y. Zhao, L. Fan, H. Wang, Z. Hou, S. Huo, N. P. Brandon, Y. Yin and M. D. Guiver, *Nature*, 2021, **595**, 361–369.

2 A. Kulkarni, S. Siahrostami, A. Patel and J. K. Nørskov, *Chem. Rev.*, 2018, **118**, 2302–2312.

3 K. Kodama, T. Nagai, A. Kuwaki, R. Jinnouchi and Y. Morimoto, *Nat. Nanotechnol.*, 2021, **16**, 140–147.

4 J. Miyake, R. Taki, T. Mochizuki, R. Shimizu, R. Akiyama, M. Uchida and K. Miyatake, *Sci. Adv.*, 2017, **3**, eaao0476.

5 J. Li, Y. Yao, L. An, S. Wu, N. Zhang, J. Jin, R. Wang and P. Xi, *Smart Mol.*, 2023, **1**, e20220005.

6 B. Jin, J. Gao, Y. Zhang and M. Shao, *Smart Mol.*, 2024, **2**, e20230026.

7 G. Shi, H. Yano, D. A. Tryk, A. Iiyama and H. Uchida, *ACS Catal.*, 2017, **7**, 267–274.

8 D. Wang, C. V. Subban, H. Wang, E. Rus, F. J. DiSalvo and H. D. Abruña, *J. Am. Chem. Soc.*, 2010, **132**, 10218–10220.

9 M. González-Hernández, E. Antolini and J. Perez, *Catalysts*, 2019, **9**, 61.

10 X. Chen, F. Niu, T. Ma, Q. Li, S. Wang and S. Shen, *Smart Mol.*, 2024, e20240056, ASAP.

11 M. Hubert, A. M. Esposito, D. Peterson, E. Miller and J. Stanford, *Hydrogen Shot: Water Electrolysis Technology Assessment*, U. S. Department of Energy, 2024.

12 D. J. Ham, Y. K. Kim, S. H. Han and J. S. Lee, *Catal. Today*, 2008, **132**, 117–122.

13 L. Szablowski, M. Wojcik and O. Dybinski, *Energy*, 2025, **316**, 134540.

14 H.-R. Pan, T. Tang, Z. Jiang, L. Ding, C. Xu and J.-S. Hu, *J. Phys. Chem. Lett.*, 2024, **15**, 3011–3022.

15 T. Takeguchi, T. Yamanaka, K. Asakura, E. N. Muhamad, K. Uosaki and W. Ueda, *J. Am. Chem. Soc.*, 2012, **134**, 14508–14512.

16 X. Yang, Y. Wang, X. Wang, B. Mei, E. Luo, Y. Li, Q. Meng, Z. Jin, Z. Jiang, C. Liu, J. Ge and W. Xing, *Angew. Chem., Int. Ed.*, 2021, **60**, 26177–26183.

17 N. Álvarez, L. R. Alden, E. Rus, H. Wang, F. J. DiSalvo and H. D. Abruña, *J. Electroanal. Chem.*, 2009, **626**, 14–22.

18 S. Gautam, A. M. K. Hadley, M. Sundarraman, S. Chugh and B. D. Gates, *ACS Appl. Energy Mater.*, 2024, **7**, 3888–3903.

19 Z. Dong, Y. Nan, T. Tang, X.-Z. Liu, J. Fu, H.-R. Pan, Z. Jiang, L. Ding, X. Cheng, L.-R. Zheng, J. Zhang, X. Chang, B. Xu and J.-S. Hu, *ACS Catal.*, 2023, **13**, 7822–7830.

20 D. Long, Y. Liu, X. Ping, F. Chen, X. Tao, Z. Xie, M. Wang, M. Wang, L. Li, L. Guo, S. Chen and Z. Wei, *Nat. Commun.*, 2024, **15**, 8105.

21 D. Shen, F. Sun, Z. Liang, B. Mei, Y. Xie, Y. Wang, L. Wang and H. Fu, *Nat. Commun.*, 2025, **16**, 3883.

22 H. Tian, X. Yu, W. Huang, Z. Chang, F. Pei, J. Zhou, N. Dai, G. Meng, C. Chen, X. Cui and J. Shi, *Small*, 2023, **19**, 2303061.

23 T. Wang, L.-Y. Li, L.-N. Chen, T. Sheng, L. Chen, Y.-C. Wang, P. Zhang, Y.-H. Hong, J. Ye, W.-F. Lin, Q. Zhang, P. Zhang, G. Fu, N. Tian, S.-G. Sun and Z.-Y. Zhou, *J. Am. Chem. Soc.*, 2022, **144**, 9292–9301.

24 C. Jin, Y. Liao, A. Zhang, S. Zhao, R. Wang, J. Li and H. Tang, *Nano Energy*, 2024, **122**, 109305.

25 B. Cai, D. Shen, Y. Xie, H. Yan, Y. Wang, X. Chen, L. Wang and H. Fu, *J. Am. Chem. Soc.*, 2024, **146**, 33193–33203.

This journal is © The Royal Society of Chemistry 2026

Catal. Sci. Technol., 2026, **16**, 101–106 | **105**

26 S. L. Scott, T. B. Gunnoe, P. Fornasiero and C. M. Crudden, *ACS Catal.*, 2022, **12**, 3644–3650.

27 Y. Yang, C. Zhao, X. Qiao, Q. Guan and W. Li, *Green Energy Environ.*, 2023, **8**, 1141–1153.

28 Z. Li, Y. Chen, S. Ji, Y. Tang, W. Chen, A. Li, J. Zhao, Y. Xiong, Y. Wu, Y. Gong, T. Yao, W. Liu, L. Zheng, J. Dong, Y. Wang, Z. Zhuang, W. Xing, C.-T. He, C. Peng, W.-C. Cheong, Q. Li, M. Zhang, Z. Chen, N. Fu, X. Gao, W. Zhu, J. Wan, J. Zhang, L. Gu, S. Wei, P. Hu, J. Luo, J. Li, C. Chen, Q. Peng, X. Duan, Y. Huang, X.-M. Chen, D. Wang and Y. Li, *Nat. Chem.*, 2020, **12**, 764–772.

29 S. J. Freakley, J. Ruiz-Esquius and D. J. Morgan, *Surf. Interface Anal.*, 2017, **49**, 794–799.

30 X. Wang, Y. Li, Y. Wang, H. Zhang, Z. Jin, X. Yang, Z. Shi, L. Liang, Z. Wu, Z. Jiang, W. Zhang, C. Liu, W. Xing and J. Ge, *Proc. Natl. Acad. Sci. U. S. A.*, 2021, **118**, e2107332118.

31 X. Wang, X. L. Yang, Y. Wang, B. B. Mei, Z. Jin, Y. Li, Z. P. Shi, Z. Jiang, C. P. Liu, W. Xing and J. J. Ge, *Sci. Bull.*, 2024, **69**, 1061–1070.

32 Y. Cong, I. T. McCrum, X. Gao, Y. Lv, S. Miao, Z. Shao, B. Yi, H. Yu, M. J. Janik and Y. Song, *J. Mater. Chem. A*, 2019, **7**, 3161–3169.

106 | *Catal. Sci. Technol.*, 2026, **16**, 101–106

This journal is © The Royal Society of Chemistry 2026